Biophysical Chemistry 125 (2007) 350–359

Biophysical Chemistry

http://www.elsevier.com/locate/biophyschem

Kinetic studies of protein L aggregation and disaggregation

Troy Cellmer [a,1], Rutger Douma [a,2], Ansgar Huebner [a,3], John Prausnitz [a,b], Harvey Blanch [a,*]

[a] Department of Chemical Engineering, University of California, Berkeley, Berkeley, CA 94720, United States
[b] Chemical Sciences Division, Lawrence Berkeley National Laboratory, Berkeley, CA 94720, United States

Received 30 August 2006; received in revised form 21 September 2006; accepted 22 September 2006
Available online 27 September 2006

Abstract

We have investigated the aggregation of protein L in 25% (vol/vol) TFE and 10 mM HCl. Under both conditions, aggregates adopt a fibrillar structure and bind dyes Congo Red and Thioflavin T consistent with the presence of amyloid fibrils. The kinetics of aggregation in 25% TFE suggest a linear-elongation mechanism with critical nucleus size of either two or three monomers. Aggregation kinetics in 10 mM HCl show a prolonged lag phase prior to a rapid increase in aggregation. The lag phase is time-dependent, but the time dependence can be eliminated by the addition of pre-formed seeds. Disaggregation studies show that for aggregates formed in TFE, aggregate stability is a strong function of aggregate age. For example, after 200 min of aggregation, 40% of the aggregation reaction is irreversible, while after 3 days over 60% is irreversible. When the final concentration of the denaturant, TFE, is reduced from 5% to 0, the amount of reversible aggregation doubles. Disaggregation studies of aggregates formed in TFE and 10 mM HCl reveal a complicated effect of pH on aggregate stability.

Keywords: Protein aggregation; Aggregation kinetics; Amyloid; Fibrils

Protein aggregation has been associated with more than twenty human diseases [1]. These diseases can be divided into two categories. In the first, the origins of disease can be traced to the aggregated protein's inability to carry out its biological function; such diseases include cystic fibrosis, Marfan syndrome, and many forms of cancer. In the second category, the protein aggregates exhibit a cytotoxic effect. Such behavior is believed to cause Alzheimer's, Parkinson's, and Huntington's diseases.

Despite the variety of proteins that form pathological aggregates, the aggregates themselves show many similarities. In many cases, they adopt a β-sheet-rich, fibrillar structure that binds dyes in a manner similar to starch (amylose) [2]. These aggregates have thus been called amyloid fibrils. However, much debate remains regarding the characteristics of the toxic aggregates. A variety of studies have suggested that precursors to the fibrillar aggregates are more toxic than the mature fibrillar aggregates [3,4], although evidence for mature-aggregate toxicity has been presented [5].

A number of recent studies has shown that proteins not associated with any known disease can form amyloid fibrils [6–8] as well as toxic aggregates [3,4]. These observations have led to the suggestion that the ability to form fibrils is a generic property of the peptide chain, and that generic mechanisms of aggregation and aggregate toxicity exist. Studies of non-disease-related proteins can be employed to determine the features of such mechanisms. For example, studies of non-disease-related proteins have shown that destabilization of the native state is the crucial factor that directs a normally soluble protein into an amyloidogenic conformation [6,9–11]. Further, the availability of a wide-range of kinetic data for the aggregation of disease and non-disease-related proteins has facilitated an attempt to rationalize protein-aggregation rates from a small number of physiochemical parameters [12]. Such an effort is very important for rational protein design, because it is helpful in narrowing the

* Corresponding author. Tel.: +1 510 642 1387.
E-mail address: blanch@berkeley.edu (H. Blanch).
[1] Laboratory of Chemical Physics, National Institute of Diabetes, Digestive, and Kidney Diseases, National Institutes of Health Bethesda, MD 20892-0520 USA.
[2] Department of Biotechnology, Delft University of Technology, Julianalaan 67, 2628 BC Delft, The Netherlands.
[3] University of Cambridge, Department of Chemistry, Lensfield Road, Cambridge, CB2 1EW UK.

0301-4622/$ - see front matter © 2006 Elsevier B.V. All rights reserved.
doi:10.1016/j.bpc.2006.09.010

search for mutations or environmental perturbations that impart an increased resistance to aggregation.

In this study, we investigate the kinetics of aggregation and disaggregation of the small α/β protein, protein L. It is comprised of 63 amino acids, and its folding properties have been addressed in detail [13]. Our motivation for studying the aggregation of protein L is two-fold. First, it is an ideal protein to study aggregation phenomena *in silico*. A minimalist model of protein L has been developed to study protein folding [14]. The computational tractability of the model has been further exploited to study aggregation phenomena [15,16]. Therefore, the experimental data presented here can be used to validate computational findings. Second, our study contributes to the effort to establish the factors responsible for protein aggregation.

Under physiological conditions, protein L forms a stable three-dimensional structure. To induce aggregation, we use 25% aqueous trifluoroethanol solutions buffered near the p*I* of the protein (pH 5.0), and conditions of low pH (10 mM HCl) coupled with high temperature (65 °C). We first present results pertaining to aggregate morphology. Next, kinetic data are reported for aggregation and disaggregation.

1. Materials and methods

1.1. Materials

Thioflavin T and 2-2-2 Trifluoroethanol (TFE) were purchased from Sigma. Sodium acetate was purchased from Fisher.

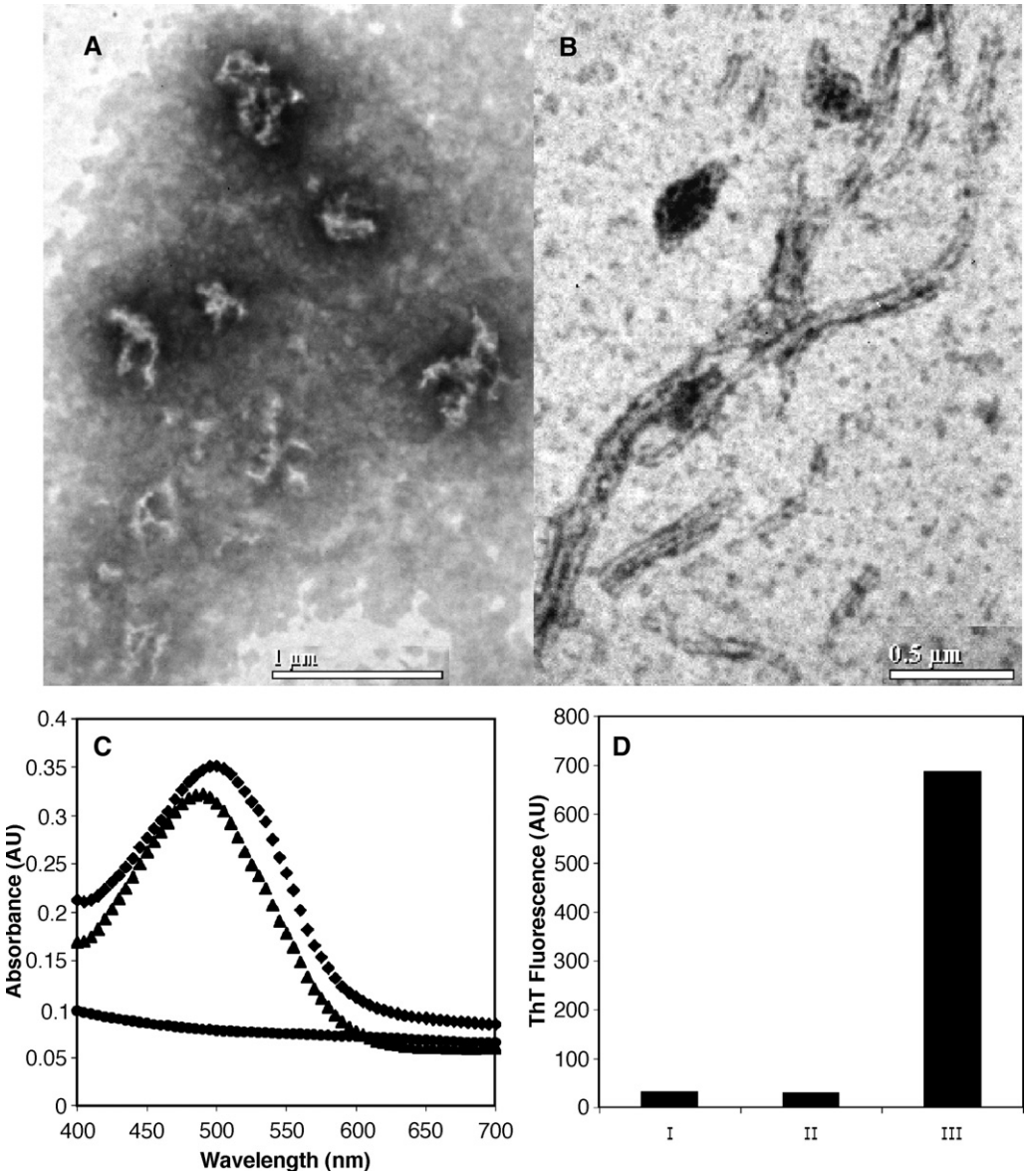

Fig. 1. (Panel A) electron micrographs of aggregates formed in 25% TFE after 5 min (left) and 24 h (right). (Panel B) absorbance spectra of buffer (circles), Congo Red in buffer (triangles), and Congo Red with protein aggregates in buffer (diamonds). Note the red shift in Congo Red absorbance. The difference in absorbance for Congo Red and Congo Red with fibrils was a maximum at 540 nm, consistent with amyloid. (Panel C) ThT fluorescence in the presence of I) protein only II) 25% TFE with 50 mM NaAc, and III) aggregates formed after 24 h in 25% TFE with 50 mM NaAc.

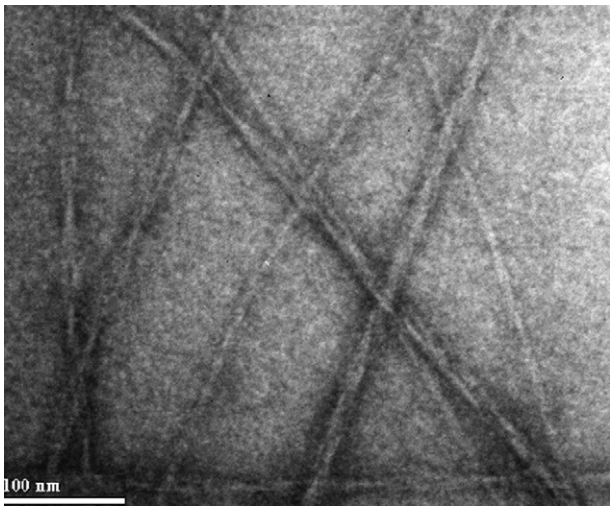

Fig. 2. Electron microscope image of amyloid fibrils formed by protein L in 10 mM HCl at 65 °C.

1.2. Protein L expression and purification

Escherichia coli strain BL21 harboring a pet15b (Novagen) plasmid encoding the sequence for protein L with six N-terminal histidine residues was obtained as a generous gift from the Baker Laboratory (University of Washington). Because the fermentation and purification protocols were essentially the same as that described in Ref. [17], only a brief description is provided here. Cell culture was carried out at the UC Berkeley Fermentation Facility. Expression of protein L was induced by addition of 0.5 mM IPTG to the growth medium. After harvesting, the cells were sonicated and the lysate centrifuged to remove cellular debris. The soluble fraction was purified using metal-chelating chromatography. After buffer exchange into water, the his-tag was cleaved by incubating CNBr in an acidic environment, and protein without the his-tag was obtained via ion-exchange chromatography. Buffer exchange was achieved using Amicon centrifuge-filter units. The purity of the protein was verified by SDS-PAGE and mass spectrometry. The protein was stored at −80 °C in single-use aliquots.

1.3. Kinetic experiments

Aggregation experiments were carried out in 50 mM sodium acetate buffer, pH 5.0 and 25% TFE, or 10 mM HCl. The temperatures of individual experiments are reported for each experiment in the Results section. The temperature was kept

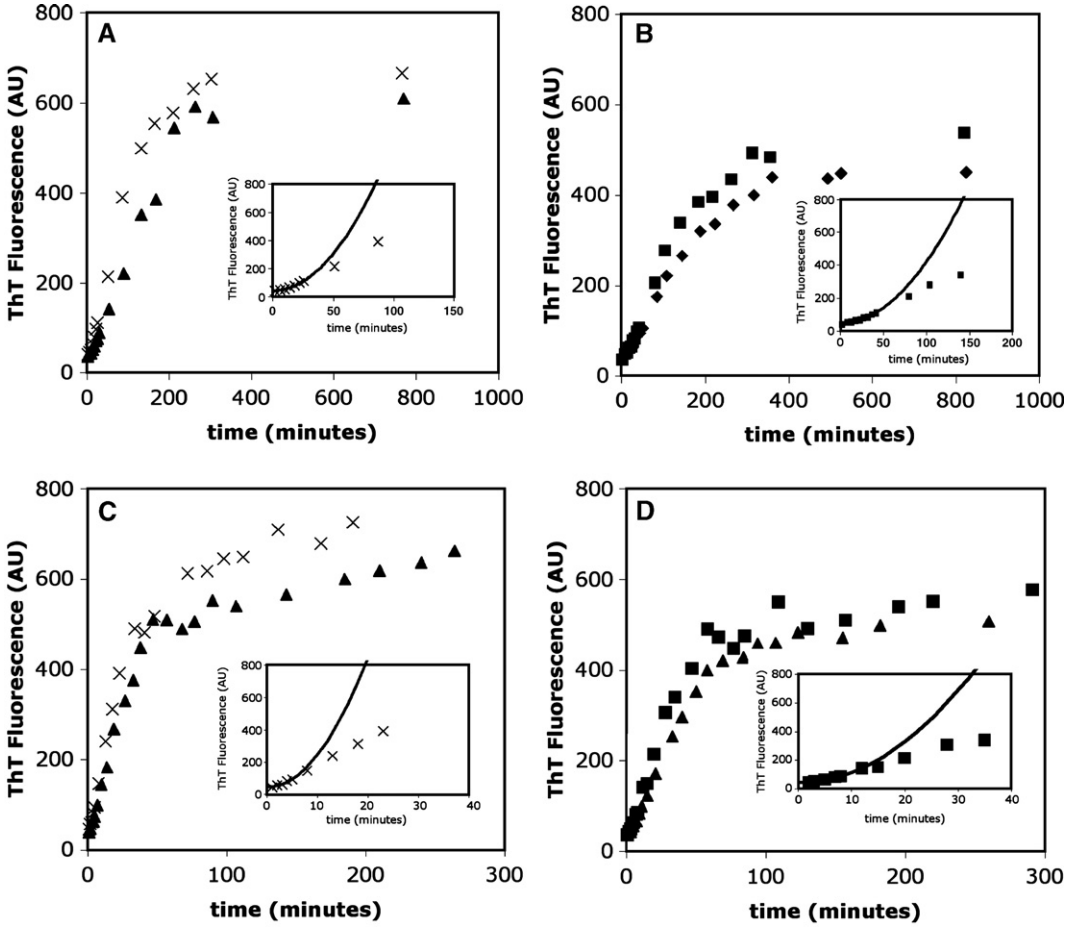

Fig. 3. Representative aggregation time courses measured from ThT fluorescence. Panel A shows time courses at 67 μM (crosses) and 59 μM (triangles) protein for solutions incubated at 20 °C. Panel B shows time courses at 55 μM (squares) and 49 μM (diamonds) protein also for solutions incubated at 20 °C. The insets in Panels A and B show t^2 fits of data for the first 10% of aggregation at protein concentrations of 67 μM and 55 μM respectively. Extra data points are shown to illustrate the flattening of the curve following the initial 10% of aggregation. Panels C and D show the same data for experiments carried out at 25 °C.

constant using a water bath. Protein solutions were syringe-filtered immediately before use and concentrations were measured spectrophotometrically. Protein-stock solutions and TFE/buffer solutions were incubated at the desired temperature for ~5 min. The protein was then added to the buffer solution to begin the experiment. Samples for ThT and electron microscope analysis were removed at times specified within the manuscript. In order to obtain representative samples, aggregation solutions were gently pipetted several times prior to sample removal.

1.4. Thioflavin T assay

Thioflavin T stock solutions were prepared by filtering a 400 μM ThT solution through a 0.2 μm Nylon Membrane syringe filter. This solution was diluted to make a working solution of 40 μM ThT and 25 mM NaH_2PO_4 pH 6.2. Throughout the ThT experiments, 20 μL samples were taken in triplicate and each added to 100 μL of ThT buffer on an opaque 96 well plate. The fluorescence of these samples was measured using a Molecular Devices Spectramax M2 platereader immediately after sample preparation. The excitation and emission wavelengths were 440 nm and 485 nm, respectively.

1.5. Congo Red assay

Aliquots of fibril-containing solutions were diluted 1:10 with 10 μM Congo Red solutions in PBS buffer (5 mM sodium phosphate, 150 mM NaCl, pH=7.4). Absorbance spectra were obtained from 400 nm to 700 nm using an AVIV Model 14NT. Spectra used to evaluate the presence of amyloid fibrils were obtained by subtracting the spectra of Congo Red in buffer and fibrils in buffer from the spectra of solutions containing buffer alone plus that of protein in the presence of Congo Red solution (see Fig. 1).

1.6. Electron microscopy

Either 2 or 4 μL aliquots of sample were placed on a carbon-coated copper grid for 2 min. The liquid was then blotted with filter paper and washed with a droplet of water. The water was

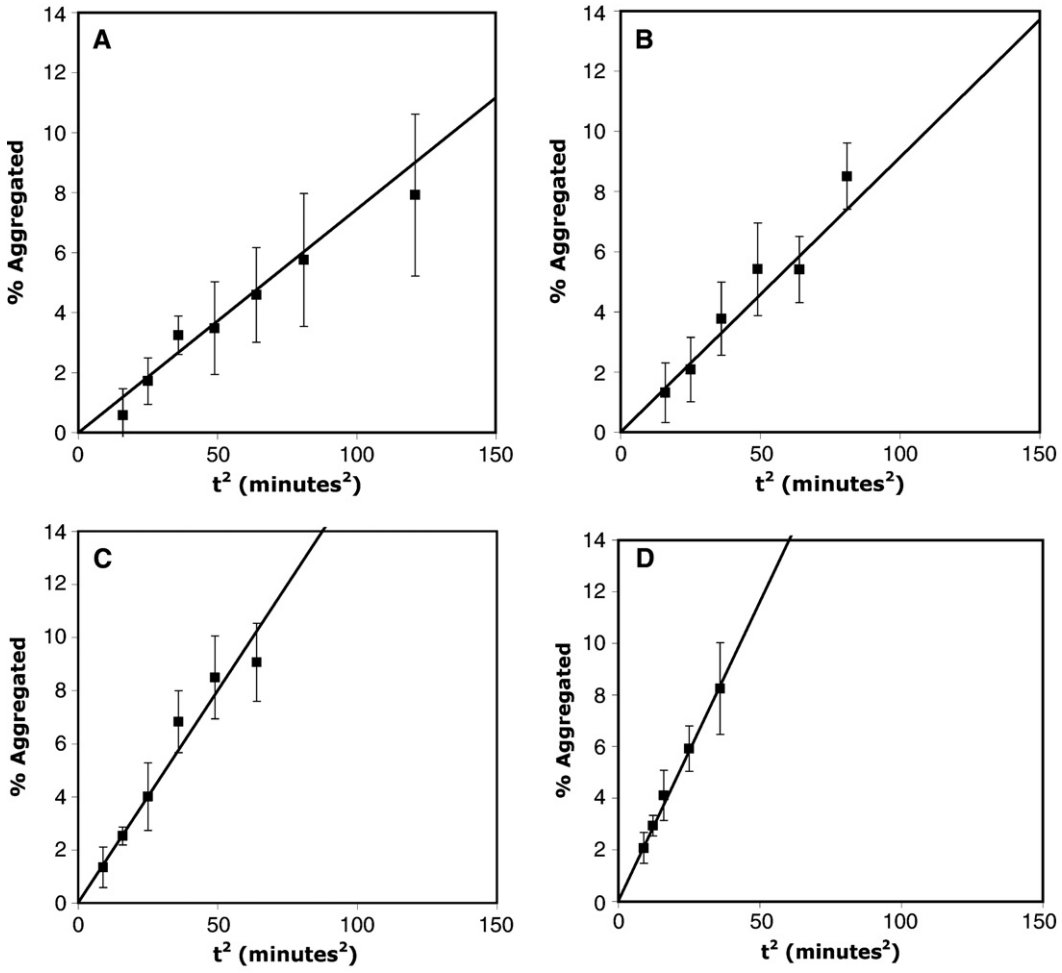

Fig. 4. Plots of θ (fraction aggregated) vs. t^2 as calculated from ThT fluorescence. Panels A, B, C, and D show data from experiments carried out at protein concentrations of 49, 55, 59, and 67 μM respectively. The temperature was 25 °C. Data points represent averages from at least 3 independent experiments, although in most cases greater than five measurements were made. The straight lines represent the best fits calculated from least-squares analysis (see Materials and methods). The R^2 values were 0.97, 0.95, 0.95, 0.99 for plots A, B, C, and D respectively. The p-values were less than 0.05.

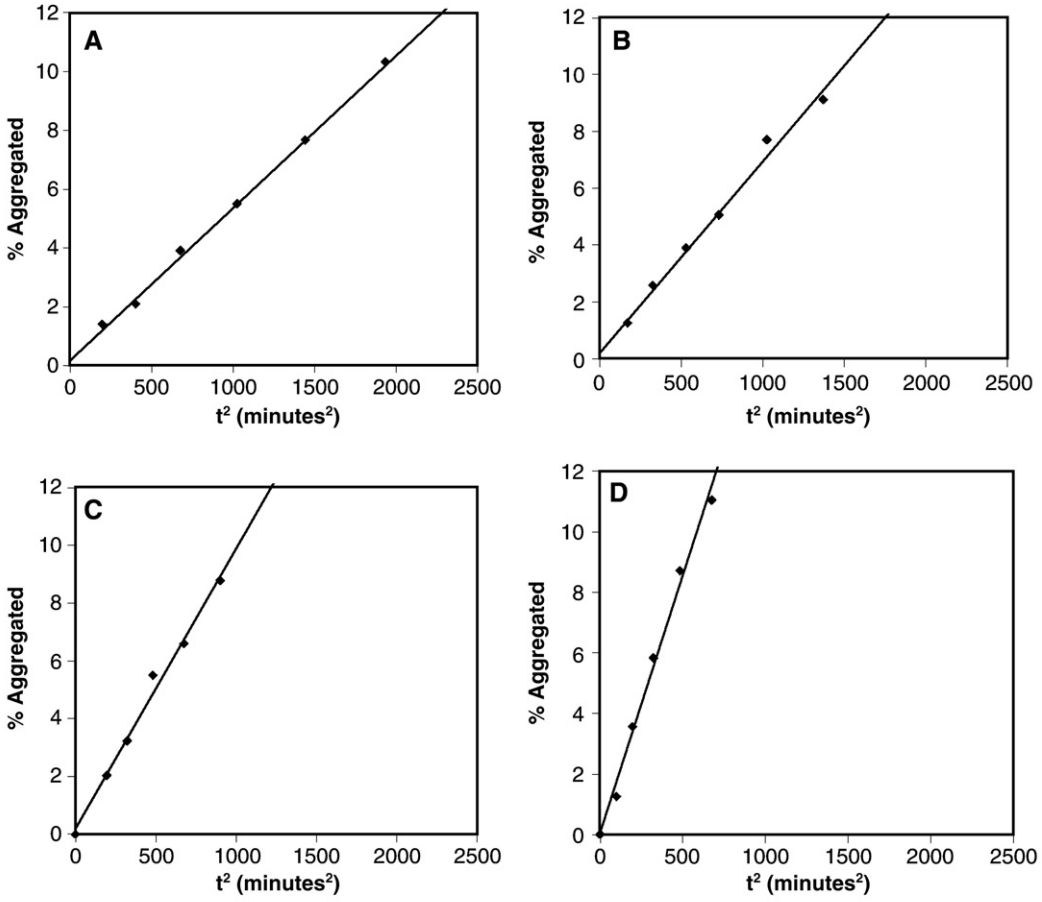

Fig. 5. Representative plots of θ (fraction aggregated) vs. t^2 as calculated from ThT fluorescence. Panels A, B, C, and D show data from experiments carried out at protein concentrations of 49, 55, 59, and 67 μM respectively. The temperature was 20 °C. The straight lines represent the best fits calculated from least-squares analysis (see Materials and methods). Typical R^2 values were >0.98. The p-values were less than 0.05.

then blotted with filter paper, and 4 μL of 2% uranyl acetate or 1% phototungstic acid was pipetted onto the grid. After 2 min, the remaining liquid was blotted with filter paper and the grid was allowed to air-dry for ~10 min. Grids were then analyzed on a Tecnai 12 transmission electron microscope at the Berkeley Electron Microscope Facility.

1.7. Modeling the early kinetics of aggregation

Based on early observations that the initial portions of aggregation time courses (in TFE) exhibited a time-squared dependence, we opted to use the linear-polymerization model proposed by Ferrone [18], later applied by Chen [19] and Ignatova [20].The rate of aggregate formation is

$$\frac{dc_A}{dt} = J^* c^* \tag{1}$$

where c_A is the concentration of aggregates, J^* is the elongation rate of nuclei, and $c*$ is the concentration of nuclei. The rate at which monomers are added to aggregates is

$$\frac{d\Delta}{dt} = Jc_A \tag{2}$$

where Δ is the concentration of monomers that have gone into aggregates and J is the elongation rate of the aggregates. The nuclei concentration is assumed to sufficiently small such that only two states are considered for each molecule, monomer or aggregate. This assumption manifests itself in the following

$$\Delta(t) = c_0 - c(t) \tag{3}$$

where c_0 is the initial concentration of monomers, c is the concentration of monomers at time t, and Δ is the concentration of aggregated material. At short times, we assume that the monomer concentration is constant. Integrating Eqs. (1) and (2) we then obtain

$$\Delta(t) = \frac{1}{2} J J^* c^* t^2 \tag{4}$$

We also assume that nuclei are elongated at the same rate as aggregates

$$J = J^* = k_e c \tag{5}$$

where k_e is the elongation rate constant. Nuclei are assumed to be in equilibrium with the bulk monomer pool, thus we obtain

$$c^* = K_n c^n \tag{6}$$

where K_n is the equilibrium coefficient and n is the nucleus size.

Using Eqs. (4) (5) and (6), we obtain

$$\Delta = \frac{1}{2} k_e^2 K_n c^{n+2} t^2 \tag{7}$$

or

$$\theta = \frac{1}{2} k_e^2 K_n c^{n+1} t^2 \tag{8}$$

where θ is the fraction aggregated. The slope of a θ vs. t^2 plot yields $\frac{1}{2} k_e^2 K_n c^{n+1}$. By plotting the logarithm of this slope against $\ln(C_0)$ we obtain a slope of the nucleus size plus one, and an intercept of $\ln\left(\frac{1}{2} k_e^2 K_n\right)$. Because the analysis is carried out on data at collected at short times, $C = C_0$.

1.8. Data analysis: early-time courses

For aggregation experiments utilizing the ThT assay, the was fraction aggregated (θ) was calculated via the following formula

$$\theta = \frac{F(t) - F_0}{F_\infty - F_0} \tag{9}$$

where $F(t)$ is the fluorescence at time t, F_0 is the background fluorescence, and F_∞ is the endpoint fluorescence. F_∞ was calculated by averaging several fluorescence measurements when the fluorescence curves had clearly reached a plateau. F_0 was calculated in each experiment through a trial-and-error procedure such that the best linear fit of the data (θ vs. t^2) passed through the origin.

For experiments conducted at 20 °C, the kinetics proceeded at a rate where a sufficient number of data points (>4) could be obtained to produce a θ vs. t^2 plot for each experiment. Linear fits to the data were obtained via a least-squares-procedure (see Fig. 2), and the uncertainty of each slope was calculated via standard procedures. At least three independent measurements were made at each concentration. The concentration dependence of these slopes yields information regarding the nucleus size. A plot of ln(slope) vs. ln(C_0) was then generated, and the data fit to a straight line through a least-squares procedure, where each data point was weighted according to its uncertainty. The uncertainty in each measurement was the sum of the standard deviation and an additional term (10% of the slope) [21] to account for the approximation of constant concentration. This plot was used to calculate the nucleus size and the quantity $k_e^2 K_N$ (Fig. 5).

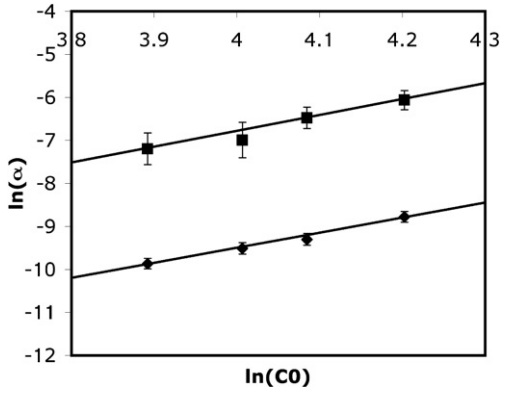

Fig. 6. Log–log plot of A (slope from θ vs. t^2 plots) vs. initial protein concentration at temperatures of 20 °C and 25 °C. The slopes from these two plots are each equal to the nucleus size (N) plus one. At 20 °C, $N = 2.47 \pm 0.47$, and at 25 °C $N = 2.83 \pm 1.31$. The intercepts are at -23.47 ± 2.20 at 20 °C and -22.27 ± 5.36 at 25 °C. The R^2 values were 0.99 and 0.96, and the p-values less than 0.05.

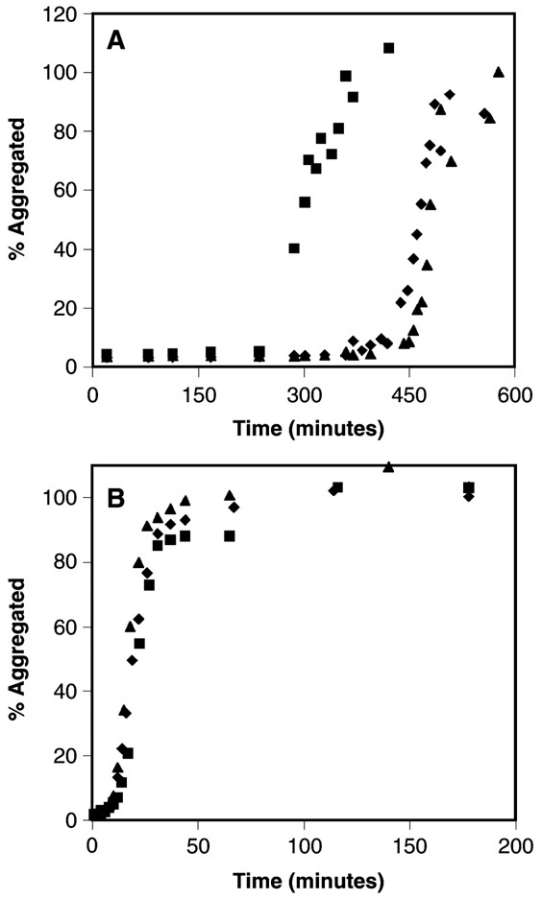

Fig. 7. Representative kinetic data for aggregation at 10 mM HCl 65 °C. Aggregation was monitored using ThT fluorescence. Panel A shows time courses from a single experiment carried out in triplicate. Panel B shows time courses for aggregation carried out in the presence of preformed fibrils. Again, the data are from a single experiment carried out in triplicate.

For experiments at 25 °C, a sufficient number of data points could not be obtained to generate a θ vs. t^2 plot for each individual experiment. The data were therefore averaged at each time point over a large number of experiments (normally >5 per condition/per time point). This averaging gave a single θ vs. t^2 plot at each concentration (see Fig. 3). These plots were fit to a straight line, where each data point was weighted according to its uncertainty.

2. Results

2.1. Aggregate morphology

First, we present data pertaining to protein L aggregation in solutions containing 25% TFE buffered at pH 5.0. Solutions containing 49 to 67 μM of protein became visibly turbid within

minutes. Aggregates formed after 5 min had a stringy appearance, as visualized by electron microscopy (Fig. 1A). After 24 h, fibrillar aggregates were observed (Fig. 1B). These solutions were further tested for the presence of amyloid fibrils using the Congo Red (Fig. 1C) and ThT assays (Fig. 1D). A red shift was observed in Congo Red absorbance, consistent with the presence of amyloid. We also observed a marked increase in ThT fluorescence in the presence of the aggregates, again indicating the presence of amyloid.

We also employed conditions of low pH (10 mM HCl) and high temperature (65 °C) to promote aggregation. After 24 h, aggregation was observed in solutions containing either 440 μM or 740 μM protein L. A larger protein concentration was used under these solution conditions to increase aggregation rates. Aggregation at lower concentrations proceeded too slowly for rigorous-kinetic study. Unlike the turbid aggregates formed in TFE, gels were formed in acidic solutions. Electron microscope images showed a dense network of fibrillar material (Fig. 2). Congo Red and Thioflavin T tests were again consistent with the presence of amyloid (data not shown).

2.2. Aggregation kinetics

Fig. 3 shows sample time courses for protein L aggregation at 20 °C and 25 °C, measured by Thioflavin T fluorescence. At all concentrations and temperatures, a lag phase was observed. The early portion of the kinetics exhibits a time-squared dependence, followed by a flattening of the curve at longer times (see inserts in Fig. 3). Both of these features are characteristic of linear aggregation [18].

Data for the first 10% of the aggregation reaction was plotted versus t^2 for each experimental condition. Fig. 4 shows representative plots for protein concentrations ranging from 49 to 67 μM at 25 °C. Because the aggregation kinetics proceed at such a rapid rate under these conditions, a large number of experiments was performed and data were averaged at each time. Each plot shows a linear dependence of the fraction of protein aggregated (θ) vs. t^2 at early times, although there are significant deviations. To verify the t^2 dependence, we reduced the temperature by 5 °C such that a sufficient number of samples could be obtained in each experiment. Again, there is a

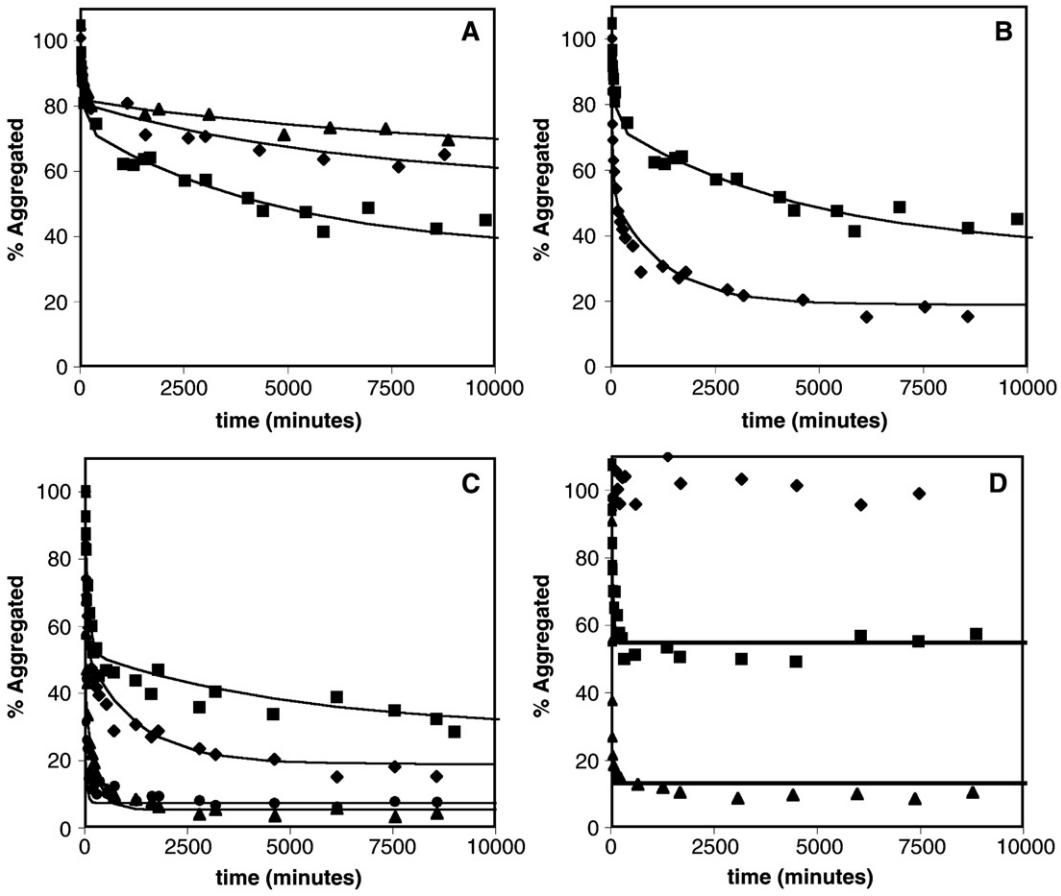

Fig. 8. Representative data from disaggregation experiments. Panels A, B, and C show disaggregation data from aggregates formed at pH 5.0 and 25% TFE. The lines in these three figures represent the best fit of the data to a bi-exponential function $F=y_0+A\exp(-k_1t)+B\exp(-k_2t)$. Panel D shows disaggregation data for aggregates formed at 10 mM HCl and 65 °C. The lines in panel D represent the best fit of the data to an single-exponential function $F=y_0+A\exp(-k_1t)$. Parameters from the fits are listed in Tables 1–4 respectively. Panel A shows data for disaggregation experiments as a function of aggregate age. Squares are from aggregates formed after 200 min, diamonds from aggregates formed after 1 day, and triangles from aggregates formed after 3 days. Panel B shows data as a function of final TFE concentration. Squares are from an experiment with a final TFE concentration of 5%, and the diamonds from an experiment with no TFE. Panel C shows data as a function of final pH. Squares represent data from pH 4.0, diamonds from pH 5.0, triangles from pH 6.0, and circles from pH 7.0.

clear linear dependence of θ vs. t^2 at early times, consistent with linear aggregation (Fig. 5).

In Figs. 4 and 5, the slopes of the plots, which we now refer to as α, can be related to the nucleus size. The nucleus size is equal to the slope of the $\ln(\alpha)$ vs. $\ln(C_0)$ plot plus one (see Materials and methods). Fig. 6 shows these plots calculated at both 20 °C and 25 °C. At both temperatures, the slopes are nearly identical, suggesting a nucleus size of either two or three monomers.

Time courses for aggregates formed in 10 mM HCl at 65 °C show a much different behavior. Four sets of kinetics experiments were conducted in triplicate for solutions containing 440 μM of protein. In one quarter of the samples, no aggregation was observed by ThT fluorescence after 24 h. When aggregation was observed, the ThT kinetics show a time dependence; the length of the lag phase varied substantially from solution to solution. Fig. 7A shows sample data from these experiments. There is a substantial period of quiescence (~hours) where no aggregation was detected by ThT fluorescence. Time-dependent aggregation kinetics have also been observed for the self-association of the Aβ-peptide and hemoglobin [22,23].

When pre-formed fibrils (at a concentration of 5% vol/vol) are added to the aggregation solution prior to the experiment, the time dependence disappears. In four independent experiments conducted in triplicate, the time required to achieve 50% aggregation had a standard deviation of less than 15%. Aggregation was observed in all samples. Fig. 7B shows a representative set of kinetic data for these experiments. As expected, the period of quiescence prior to a detectable aggregation signal is substantially reduced. In these experiments, all solutions showed a detectable increase in ThT fluorescence within minutes after the experiment began.

2.3. Reversibility of aggregation

The reversibility of the aggregation process was studied as a function of aggregate age, the presence of TFE, and final solution pH. The reversibility was tested by either diluting or removing the denaturant, and following the decrease in ThT fluorescence of the solution. In each case, controls were performed where the aggregates were simply diluted into the aggregating solution. In these experiments, there was no decrease in ThT fluorescence beyond that associated with lowering the concentration of aggregates.

Table 1
Disaggregation rates and amplitudes as a function of aggregate age

	200 min	24 h	72 h
y_0 t_∞ amplitude	0.40 (0.08)	0.56 (0.01)	0.63 (0.02)
A fast phase amp.	0.27 (0.05)	0.19 (0.02)	0.18 (0.02)
k_1 fast phase rate	0.013 (0.001)	0.03 (0.01)	0.013 (0.003)
B slow phase amp.	0.32 (0.08)	0.25 (0.01)	0.18 (0.02)
k_2 slow phase rate	0.0002 (0.0001)	0.0002 (0.0001)	0.0001 (0.0001)

Aggregates were formed in 25% TFE and 50 mM sodium acetate pH 5.0. The standard deviation from at least three independent measurements is listed in parentheses next to each parameter value. The amplitudes have no units, and are presented as a fraction of the ThT fluorescence at $t=0$. The rates are in units of 1/min. See also Fig. 8, Panel A.

Table 2
Disaggregation rates and amplitudes as a function of final TFE concentration

	0%	5%
y_0 t_∞ amplitude	0.19 (0.01)	0.40 (0.08)
A fast phase amp.	0.46 (0.01)	0.27 (0.05)
k_1 fast phase rate	0.03 (0.01)	0.013 (0.001)
B slow phase amp.	0.34 (0.01)	0.32 (0.08)
k_2 slow phase rate	0.0007 (0.0001)	0.0002 (0.0001)

Aggregates were formed in 25% TFE and 50 mM sodium acetate pH 5.0. The standard deviation from at least three independent measurements is listed in parentheses next to each parameter value. The amplitudes have no units, and are presented as a fraction of the ThT fluorescence at $t=0$. The rates are in units of 1/min. See also Fig. 8, Panel B.

Fig. 8A shows disaggregation time courses as a function of aggregation age. Solutions containing protein L at 67 μM, 25% TFE, and 50 mM sodium acetate pH 5.0 were allowed to incubate for 200 min, 24 h, or 72 h. The aggregate solution was diluted five-fold with acetate buffer and ThT fluorescence was monitored. For all three conditions the data were best fit by a double-exponential function. Table 1 shows the parameters from the fits. The ThT signal at infinite time (y_0) increases with aggregate age, indicating that the reversibility of aggregation is inversely correlated to the time the protein spends in the denaturant. The amplitudes of both the fast (A) and slow (B) phases decrease when aggregates are allowed to age for 24 h. For 72 hour samples, only the slow-phase amplitude decreases further. The slow-phase rates (k_2) are all the same within experimental error. The fast-phase rate (k_1) is larger for samples incubated for 24 h than those incubated for 200 min or 72 h.

In the above experiments, aggregates were diluted five-fold into acetate buffer leaving some denaturant (5% TFE). In a second set of experiments, we tested the effect of this remaining denaturant on aggregate stability by centrifuging the aggregates after 200 min, removing the liquid phase, and then diluting with acetate buffer. The liquid phase gave only background ThT fluorescence, showing that essentially all the aggregates were removed during centrifugation. Fig. 8B shows sample time

Table 3
Disaggregation rates and amplitudes as a function of final pH

	4.0	5.0	6.0	7.0
y_0 t_∞ amplitude	0.31 (0.02)	0.19 (0.01)	0.06 (0.01)	0.11 (0.06)
A fast phase amp.	0.43 (0.05)	0.46 (0.01)	0.63 (0.10)	0.64 (0.05)
k_1 fast phase rate	0.02 (0.02)	0.03 (0.01)	0.06 (0.02)	0.34 (0.12)
B slow phase amp.	0.26 (0.03)	0.34 (0.01)	0.32 (0.10)	0.25 (0.04)
k_2 slow phase rate	0.0003 (0.0001)	0.0007 (0.0001)	0.004 (0.002)	0.02 (0.01)

Aggregates were formed in 25% TFE and 50 mM sodium acetate pH=5.0. The standard deviation from at least three independent measurements is listed in parentheses next to each parameter value. The amplitudes have no units, and are presented as a fraction of the ThT fluorescence at $t=0$. The rates are in units of 1/min. See also Fig. 8, Panel C.

Table 4
Disaggregation rates and amplitudes as a function of final pH

	5.0	7.0
y_0 t_∞ amplitude	0.56 (0.06)	0.18 (0.04)
A amplitude	0.44 (0.06)	0.82 (0.04)
k_1 rate	0.03 (0.02)	0.11 (0.04)

The standard deviation from at least three independent measurements is listed in parentheses next to each parameter value. Aggregates were formed in 10 mM HCl at 65 °C. The amplitudes have no units, and are presented as a fraction of the ThT fluorescence at $t=0$. The rates are in units of 1/min. See also Fig. 8, Panel D.

courses and Table 2 shows parameters from bi-exponential fits to the data. Even though 5% TFE is insufficient to initiate aggregation (data not shown), it clearly has an effect on the stability of the aggregates. The constant y_0 doubles in the presence of TFE, showing that even small amounts of TFE have a stabilizing effect. The majority of this increase comes at the expense of the fast-phase amplitude, while the slow-phase amplitudes are nearly identical. Both fast and slow-phase rates are nearly tripled if all TFE is removed from the refolding solution.

We also studied the reversibility of the aggregation process as a function of pH. Aggregates formed at pH 5.0, 25% TFE, and 25 °C were centrifuged after 200 min. The buffer was removed and replaced by fresh buffer at a pH of 4.0, 5.0, 6.0, or 7.0. For solutions at pH 4.0 and 5.0, 50 mM acetate was used, while at pH 6.0 and 7.0 50 mM phosphate was used. The ThT signal was then monitored as in previous experiments. All data sets were best fit by a bi-exponential function. Fig. 8C shows representative time courses, and Table 3 gives the parameters from the bi-exponential fits.

The value of y_0 with decreasing pH from pH 6.0 to 4.0. The value at pH 7.0 is within the experimental error of that at pH 6.0. The fast-phase amplitudes show the opposite trend, while there is no clear trend in the slow-phase amplitudes. Both the slow and fast-phase rates increase with rising pH.

Lastly, we present data pertaining to the stability of aggregates formed at low pH and high temperature. Because of the irreproducibility of the aggregation process without seeding, aggregation solutions were seeded with pre-formed fibrils; for disaggregation studies, after 200 min, aliquots of these solutions were diluted in buffers containing, 10 mM HCl, 50 mM sodium acetate pH 5.0, or sodium phosphate pH 7.0. In this case, the data were best fit by a single-exponential function. Fig. 8D shows sample time courses, and Table 4 shows the parameters from the single-exponential fits. Control data show that when the aggregates are diluted into 10 mM HCl, there is no change in ThT fluorescence over the length of the experiment. There is a large decrease in the value of y_0 when the pH rises from 5.0 to 7.0, corresponding to a large decrease in aggregate stability. The disaggregation rate increases by nearly a factor of four.

3. Discussion

We have studied the aggregation of protein L under denaturing conditions. Solutions of 25% TFE and 10 mM HCl promote the formation of amyloid fibrils, as observed from electron microscopy and from Congo Red and Thioflavin T assays. Our results support the hypothesis that the ability to form amyloid is a generic property of all proteins [6].

When 25% TFE is used as a denaturant, the time courses exhibit behavior characteristic of a nucleated linear-polymerization. The concentration dependence of the rates suggests that the nucleus size is on the order of 2–3 monomers. In 10 mM HCl, the situation is less clear. There is a time-dependence for the substantial lag phase that precedes aggregation. It is not apparent if this time dependence is due to our intrusive sampling protocol, which requires that the solution be disturbed for sample collection, or some stochastic aggregation event. Further study will be required to resolve this issue. However, the disparate characteristics of the time courses strongly suggest that the aggregation mechanisms under the two conditions are different.

Disaggregation experiments show that for aggregates formed in TFE, both the aggregate age and the remaining denaturant play a large role in determining aggregate stability. Using a similar experimental system (25% TFE as a denaturant) and protocol similar to that employed here, Calamai et al. [25] showed that acylphosphatase disaggregation slows as aggregates age and the percentage of irreversible aggregates increases with aggregate age. We observe a similar trend in irreversibility with aggregate age. Calamai [25] also observed bi-phasic kinetics for disaggregation experiments. The different phases were correlated with aggregate size; larger aggregates disaggregated more slowly. It would be interesting to see if this is this case for protein L disaggregation.

We have shown that aggregate stability is a strong function of pH for aggregates formed either in TFE or acid. Side-chain-titration data suggest that the pI of protein L is 4.9. For aggregates formed in TFE, the stability decreases as the pH rises from 5.0 to 7.0. Assuming that the estimate of pI=4.9 is accurate, it might be argued that the increase in net charge is responsible for the loss of stability. Net charge has been shown to be a strong factor in determining aggregation rates [12]. However, there is also a significant stability increase from pH 5.0 to 4.0, where the net charge would again be expected to increase. It is possible that the estimate of the pI is not accurate. Further experiments, such as looking more closely at stabilities between pHs 4.0 and 5.0 may add additional insight to this problem.

The stability of aggregates formed in 10 mM HCl is also compromised when exposed to solutions of different pH. In this case, there is clearly a decrease in aggregate stability with a decrease in net charge. Presumably, low pH conditions give rise to amyloid formation because of the destabilizing effect on the native state. Therefore, the increased stability of the native state encountered under the refolding conditions employed here would shift the equilibrium in that direction. However, the y_0 value at pH 5.0 is more than triple that at pH 7.0. It would be somewhat surprising for any modest native-state stability differences under the two conditions to promote such a large difference in aggregate stability. One possible explanation for such a dramatic change is that one or several of protein L's ten

acidic side chains could be required for aggregate stability. It is feasible that such an amino acid(s) may not be charged at pH 5.0, but would be at pH=7.0. However, barring a high-resolution structure of the fibril, such a hypothesis would be difficult to verify experimentally. Molecular simulation would be helpful in resolving this issue.

The data from these experiments provide guidance in designing novel computational studies. It should be possible to adjust the potential functions used in simulating coarse-grained model proteins to roughly mimic the solution conditions used in our study. While quantitative comparison may be difficult, simulations should be able to offer some new insight into the aggregation mechanisms. Protein L is an ideal test candidate for such simulations; [14] have developed a coarse-grained model that reproduces characteristics of its folding pathway. Computational tractability has been established making the model optimal for simulations of aggregation [16,24]. It would be interesting to see if these models, with some minor changes to the potential function, could shed light why the two different solution conditions studied here promote such different aggregation behavior. Similarly intriguing is the possibility that the simulations may offer testable hypotheses for aggregation abatement. Identification of amino-acid substitutions that prevent aggregation is one approach that is experimentally testable. Molecular-level insight into the means by which mutations, as well as alterations to solution conditions, affect aggregation pathways may also be utilized to refine empirical approaches for predicting aggregation rates.

Acknowledgement

For financial support, the authors are grateful to the National Science Foundation and to the Office for Basic Energy Sciences of the U.S. Department of Energy.

References

[1] M. Stefani, C.M. Dobson, Protein aggregation and aggregate toxicity: new insights into protein folding, misfolding diseases and biological evolution, J. Mol. Med. 81 (2003) 678–699.
[2] C. Dobson, The structural basis of protein folding and its links with human disease, Philos. Trans. R. Soc. Lond., B 356 (2001) 133–145.
[3] M. Bucciantini, G. Calloni, F. Chiti, L. Formigli, D. Nosi, C.M. Dobson, M. Stefani, Prefibrillar amyloid protein aggregates share common features of cytotoxicity, J. Biol. Chem. 279 (2004) 31374–31382.
[4] M. Bucciantini, E. Giannoni, F. Chiti, F. Baroni, L. Formigli, J. Zurdo, N. Taddei, G. Ramponi, C.M. Dobson, M. Stefani, Inherent toxicity of aggregates implies a common mechanism for protein misfolding diseases, Nature 416 (2002) 507–511.
[5] a.T. Petkova, R.D. Leapman, Z.H. Guo, W.M. Yau, M.P. Mattson, R. Tycko, Self-propagating, molecular-level polymorphism in Alzheimer's beta-amyloid fibrils, Science 307 (2005) 262–265.
[6] F. Chiti, P. Webster, N. Taddei, A. Clark, M. Stefani, G. Ramponi, C. Dobson, Designing conditions for in vitro formation of amyloid protofilaments and fibrils, Proc. Natl. Acad. Sci. U. S. A. 96 (1999) 3590–3594.
[7] M. Ramirez-Alvarado, J.S. Merkel, L. Regan, A systematic exploration of the influence of the protein stability on amyloid fibril formation in vitro, Proc. Natl. Acad. Sci. U. S. A. 97 (2000) 8979–8984.
[8] J. Zurdo, J.I. Guijarro, J.L. Jimenez, H.R. Saibil, C.M. Dobson, Dependence on solution conditions of aggregation and amyloid formation by an SH3 domain, J. Mol. Biol. 311 (2001) 325–340.
[9] D. Hamada, C.M. Dobson, A kinetic study of beta-lactoglobulin amyloid fibril formation promoted by urea, Protein Sci. 11 (2002) 2417–2426.
[10] A. Fink, Protein aggregation: folding aggregates, inclusion bodies, and amyloid, Fold. Des. 3 (1998) R9–R23.
[11] J. Goers, S.E. Permyakov, E.A. Permyakov, V.N. Uversky, A.L. Fink, Conformational prerequisites for alpha-lactalbumin fibrillation, Biochemistry 41 (2002) 12546–12551.
[12] K.F. DuBay, A.P. Pawar, F. Chiti, J. Zurdo, C.M. Dobson, M. Vendruscolo, Prediction of the absolute aggregation rates of amyloidogenic polypeptide chains, J. Mol. Biol. 341 (2004) 1317–1326.
[13] D. Kim, C.F., D. Baker, A breakdown of symmetry in the folding transition state of protein L. J. Mol. Biol. 298 (2000) 971–984.
[14] J. Sorenson, T. Head-Gordon, Protein engineering study of protein L by simulation, J. Comput. Biol. 9 (2002) 35–54.
[15] N.L. Fawzi, V. Chubukov, L.A. Clark, S. Brown, T. Head-Gordon, Influence of denatured and intermediate states of folding on protein aggregation (vol 14, pg 993, 2005), Protein Sci. 14 (2005) 1380-1380.
[16] L.A. Clark, Protein aggregation determinants from a simplified model: cooperative folders resist aggregation, Protein Sci. 14 (2005) 653–662.
[17] H.D. Gu, Q.a. Yi, S.T. Bray, D.S. Riddle, a.K. Shiau, D. Baker, A phage display system for studying the sequence determinants of protein-folding, Protein Sci. 4 (1995) 1108–1117.
[18] F. Ferrone, Analysis of protein aggregation kinetics, Amyloid, Prions, and Other Protein Aggregates, vol. 309, 1999, pp. 256–274.
[19] S.M. Chen, F.A. Ferrone, R. Wetzel, Huntington's disease age-of-onset linked to polyglutamine aggregation nucleation, Proc. Natl. Acad. Sci. U. S. A. 99 (2002) 11884–11889.
[20] Z. Ignatova, L.M. Gierasch, Aggregation of a slow-folding mutant of a beta-clam protein proceeds through a monomeric nucleus, Biochemistry 44 (2005) 7266–7274.
[21] M.F. Bishop, F.a. Ferrone, Kinetics of nucleation-controlled polymerization— a perturbation treatment for use with a secondary pathway, Biophys. J. 46 (1984) 631–644.
[22] P. Hortschansky, V. Schroeckh, T. Christopeit, G. Zandomeneghi, M. Fandrich, The aggregation kinetics of Alzheimer's beta-amyloid peptide is controlled by stochastic nucleation, Protein Sci. 14 (2005) 1753–1759.
[23] J. Hofrichter, Kinetics of sickle hemoglobin polymerization. III. Nucleation rates determined from stochastic fluctuations in polymerization progress curves, J. Mol. Biol. 189 (1986) 553–571.
[24] N.L. Fawzi, V. Chubukov, L.A. Clark, S. Brown, T. Head-Gordon, Influence of denatured and intermediate states of folding on protein aggregation, Protein Sci. 14 (2005) 993–1003.
[25] M. Calamai, C. Canale, A. Relini, M. Stefani, F. Chiti, C.M. Dobson, Reversal of protein aggregation provides evidence for multiple aggregated States, J. Mol. Biol. 346 (2005) 603–616.